

Vortex lattice disorder in $\text{YBa}_2\text{Cu}_3\text{O}_{7-\delta}$ probed using β -NMR

H. Saadaoui,¹ W. A. MacFarlane,² Z. Salman,^{3,*} G. D. Morris,³ Q. Song,¹ K. H. Chow,⁴ M. D. Hossain,¹ C. D. P. Levy,³ A. I. Mansour,⁴ T. J. Parolin,² M. R. Pearson,³ M. Smadella,¹ Q. Song,¹ D. Wang,¹ and R. F. Kieffl,^{1,3,5}

¹*Department of Physics and Astronomy, University of British Columbia, Vancouver, BC, Canada, V6T 1Z1*

²*Chemistry Department, University of British Columbia, Vancouver, BC, Canada, V6T 1Z1*

³*TRIUMF, 4004 Wesbrook Mall, Vancouver, BC, Canada, V6T 2A3*

⁴*Department of Physics, University of Alberta, Edmonton, AB, Canada, T6G 2G7*

⁵*Canadian Institute for Advanced Research, Toronto, Canada M5G 1Z8*

β -detected NMR (β -NMR) has been used to study vortex lattice disorder near the surface of the high- T_C superconductor $\text{YBa}_2\text{Cu}_3\text{O}_{7-\delta}$ (YBCO). The magnetic field distribution from the vortex lattice was detected by implanting a low energy beam of highly polarized $^8\text{Li}^+$ into a thin overlayer of silver on optimally doped, twinned and detwinned YBCO samples. The resonance in Ag broadens significantly below the transition temperature T_C as expected from the emerging field lines of the vortex lattice in YBCO. However, the lineshape is more symmetric and the dependence on the applied magnetic field is much weaker than expected from an ideal vortex lattice, indicating that the vortex density varies across the face of the sample, likely due to pinning at twin boundaries. At low temperatures the broadening from such disorder does not scale with the superfluid density.

PACS numbers: 74.72.-h, 74.25.Qt, 75.60.-K, 75.70.Cn

I. INTRODUCTION

The vortex state of cuprate superconductors is of central importance in understanding high- T_C superconductivity (HTSC). One of the most well studied quantities is the internal magnetic field distribution $p(B)$ associated with the vortex lattice (VL).¹⁻⁴ As discussed below, several methods can be used to measure $p(B)$, which depends on the London penetration depth λ , the coherence length ξ ,^{5,6} and, to a lesser extent, the internal structure of the vortices,⁷ and non-linear and non-local effects.^{4,8,9} The form of $p(B)$ has a distinctive asymmetric shape due to the spatial magnetic inhomogeneity characteristic of an ordered two-dimensional (2D) lattice of vortices. One basic feature in $p(B)$ is a prominent high field tail associated with the vortex cores, which depends on the magnitude of ξ . There is also a saddle point in the local field profile located between two vortices. This gives rise to a Van Hove singularity or sharp peak in $p(B)$ below the average field. The overall width or second moment of $p(B)$ depends primarily on the London penetration depth λ , the lengthscale over which the magnetic field is screened. Anisotropy of the Fermi surface or the superconducting order parameter can result in a different VL but the main features are similar for any ordered lattice.^{10,11}

Another general feature associated with any real VL is disorder arising from vortex pinning at structural defects and impurities.^{12,13} Structural defects are present in all superconductors to some degree, but may be more prevalent in structurally complex compounds such as YBCO. For example, YBCO's slightly orthorhombic structure facilitates crystal twinning, i.e. in a single crystal, there are generally domains with the nearly equal a and b directions interchanged. Separating such twin domains are well defined 45° grain boundaries or twin boundaries which have been shown to be effective extended vortex pinning sites.¹⁴⁻¹⁷ Scanning tunneling

microscopy (STM) imaging of a twinned YBCO crystal show that the areal vortex density is strongly modified by the twin boundaries.¹⁸ Small-angle neutron scattering (SANS) studies of YBCO confirm that the twin boundaries strongly deform the VL.^{15,19} Understanding the influence of such structural defects on the VL has been the subject of intense theoretical work,²⁰⁻²² and is important for two main reasons. Firstly, it affects $p(B)$ and thus adds uncertainty to measurements of fundamental quantities like λ and ξ , since it can be difficult to isolate such extrinsic effects from changes in fundamental quantities of interest. Secondly, the degree of pinning of vortices determines the critical current density which is important for many applications.²³

Measurements of the vortex state field distribution $p(B)$ are most often done using SANS,^{15,19} nuclear magnetic resonance (NMR),²⁴ and conventional muon-spin rotation (μSR).²⁵ All these methods probe the VL in the bulk and can be applied over a wide range of magnetic fields. It is also possible to probe the magnetic field distribution $p(B)$ near the surface of the sample using low energy- μSR (LE- μSR) in low magnetic fields.²⁶ Recently we have demonstrated that similar information on $p(B)$ near a surface can be obtained using β -NMR.² This has the advantage that it can be applied over a wide range of magnetic fields.

In this paper, we report measurements of the VL above the surface of the cuprate superconductor $\text{YBa}_2\text{Cu}_3\text{O}_{7-\delta}$ using β -NMR.²⁷⁻³² The $^8\text{Li}^+$ beam was implanted into a thin silver overlayer evaporated onto several YBCO samples. Measuring in the Ag allows one to isolate the contribution to $p(B)$ from *long wavelength disorder*, i.e. disorder that occurs on length scales much longer than the vortex spacing and λ due to structural defects such as twin and grain boundaries. This is possible because the field distribution broadening just outside the superconductor due to the VL inside has a very distinctive field

dependence. In particular, it vanishes in high magnetic fields where the VL spacing becomes less than the characteristic distance of the probe from the superconductor. On the other hand, long wavelength disorder has a much weaker dependence on magnetic field and dominates the observed $p(B)$ in the high field limit. Our results show evidence for significant broadening of $p(B)$ from such long wavelength disorder on the scale of $D \approx 1 \mu\text{m}$, which is attributed to pinning at twin or other grain boundaries. The magnitude of the broadening is similar to that observed in bulk μSR measurements, suggesting that the same broadening contributes to $p(B)$ in bulk μSR measurements. There is a crossover such that near T_C , where $\lambda \gg D$, the broadening scales with the superfluid density, whereas at lower temperatures, where $\lambda \ll D$, the broadening does not track the superfluid density. We discuss the consequences of this for the inference of $\lambda(T)$ from measurements of $p(B)$ in polycrystalline superconductors.

The paper is organized as follows: section II reviews the theory for the field distribution, and its second moment near the surface of a superconductor. Section III contains all the experimental details. In Section IV, we present the results. Finally in section V we discuss the results and draw conclusions.

II. THE MAGNETIC FIELD DISTRIBUTION $p(B)$ IN THE VORTEX STATE

In a type II superconductor, above the lower critical field B_{c1} , the magnetic field penetrates the sample *inhomogeneously* forming a lattice of magnetic vortices, each carrying a flux quantum, $\Phi_0 = h/2e$. In a perfect crystal, intervortex interactions lead to a long-range ordered 2D lattice of vortices, usually of triangular (hexadic) symmetry.¹ At the core of each vortex (a cylinder of radius approximately the superconductor's coherence length ξ), the local magnetic field is maximal. Outside the core, concentric circulating supercurrents partially screen the field which thus falls exponentially with a lengthscale λ . The average magnetic field in the VL is the applied field B_0 for flat samples, where demagnetization effects are negligible.³³⁻³⁵ At a given field, the average vortex spacing, i.e. the lattice constant of the VL, a is fixed. For the triangular lattice this is

$$a = \sqrt{\frac{2\Phi_0}{\sqrt{3}B_0}} \approx \frac{1546 \text{ nm}}{\sqrt{B_0(\text{mT})}}. \quad (1)$$

If one considers the profile of the magnetic field along a line in the lattice (perpendicular to the direction of the applied field), it is thus *corrugated* with a period determined by a . This inhomogeneity in the magnetic field causes a characteristic broadening in local magnetic resonance probes such as the muons in μSR or the host nuclei in NMR. Since the muon (or host nuclear spin) is at a well-defined lattice site(s), it samples the VL with a grid

spacing given by the lattice constant of the crystal. Since this is much smaller than the VL constant, the resulting field distribution $p(B)$ provides a random sampling of the spatially inhomogeneous field $B(r)$ over the VL unit cell:

$$p(B) = \frac{1}{A} \int_A \delta(B - B(r)) dr, \quad (2)$$

where the integral is over a unit cell of the VL of area A . In this paper we are concerned with the z -component of the magnetic field B_z (parallel to the c -axis of YBCO samples), and refer to it simply as B .

For an ideal triangular VL, the spatial dependence of the z -component of the magnetic field in or outside a type II superconductor follows the modified London equation,

$$-\nabla^2 B - \frac{\partial^2 B}{\partial z^2} + \frac{B}{\lambda^2} \Theta(z) = \frac{\Phi_0}{\lambda^2} \Theta(z) \sum_{\mathbf{R}} \delta(\mathbf{r} - \mathbf{R}). \quad (3)$$

Here $\lambda = \lambda_{ab}$ when the applied field is along the c -axis and the screening supercurrents flow in the ab plane, ∇^2 is the 2D Laplacian, $\Theta(z) = 1$ for $z > 0$ and zero otherwise, \mathbf{r} is a 2D vector in the xy plane, \mathbf{R} are the Bravais lattice vectors for the VL. We define the z axis as the normal to the surface of a superconducting slab with negative z outside the superconductor. The solution of Eq. (3) is easily obtained using the Fourier transform, $B(\mathbf{r}, z) = B_0 \sum_{\mathbf{k}} e^{i\mathbf{k}\cdot\mathbf{r}} F(\mathbf{k}, z)$, where the dimensionless Fourier components, $F(\mathbf{k}, z)$, are given by,³⁶

$$F(\mathbf{k}, z) = \frac{1}{\lambda^2} \left[\frac{\Theta(-z)e^{kz}}{\Lambda(\Lambda + k)} + \frac{\Theta(z)}{\Lambda^2} \left(1 - \frac{k}{\Lambda + k} e^{-\Lambda z} \right) \right]. \quad (4)$$

Here $\Lambda^2 = k^2 + \frac{1}{\lambda^2}$, and $\mathbf{k} = \frac{2\pi}{a} [n\mathbf{x} + \frac{2m-n}{\sqrt{3}}\mathbf{y}]$ are the reciprocal lattice vectors of the triangular VL, where $m, n = 0, \pm 1, \pm 2, \dots$. A cutoff function $C(k)$, approximated by a simple Gaussian $C(k) \approx e^{-\frac{\xi^2 k^2}{2}}$, can be used to account for the finite size of the vortex core, where $F(\mathbf{k}, z)$ is replaced by $F(\mathbf{k}, z)C(k)$.^{2,4} However, the corrections due to $C(k)$ are very small in our case, so it will be omitted. An approximate solution for the magnetic field along z (both inside and outside the superconductor) is given by

$$B(\mathbf{r}, z) = B_0 \sum_{\mathbf{k}} F(\mathbf{k}, z) \cos(\mathbf{k} \cdot \mathbf{r}). \quad (5)$$

The second moment of $p(B)$ at a depth z , $\sigma^2 = \langle B^2 \rangle - \langle B \rangle^2$, where $\langle \dots \rangle$ is the spatial average, is given by

$$\sigma^2 = B_0^2 \sum_{\mathbf{k} \neq 0} F^2(\mathbf{k}, z). \quad (6)$$

The field distribution for a perfectly ordered triangular VL calculated from Eqs. (2) and (5), at $B_0 = 52 \text{ mT}$ and outside the superconductor at $z = -90 \text{ nm}$ and $\lambda = 150 \text{ nm}$ (relevant to YBCO at $T \ll T_C$), is presented in Fig. 1(a) ($\Delta_D = 0$, defined below). It shows

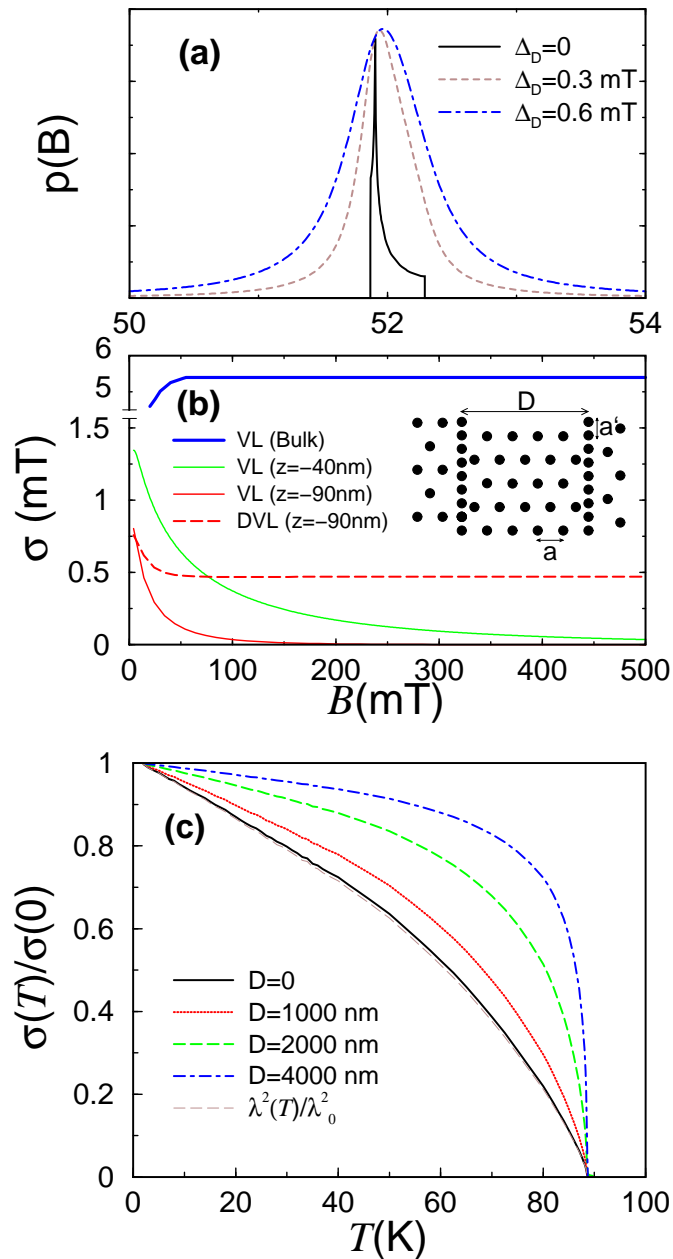


FIG. 1: (Color online) (a) Simulation of $p(B)$ in an applied field of 52 mT at a distance 90 nm from the superconductor using Eq. (5) convoluted with a Lorentzian of width Δ_D . (b) The broadening of $p(B)$ versus the applied field. Solid lines represent σ from Eq. (6) in the bulk, and 40 and 90 nm away from the superconductor. Long dashed line shows σ at 90 nm from Eq. (9) for $D = 4 \mu\text{m}$ and $f = 0.1$. Inset: sketch of a possible vortex arrangement including vortex trapping at twin boundaries spaced by D and a regular triangular vortex lattice elsewhere. (c) $\sigma(T)$ (normalized at $T = 0$), from Eq. (9) for $B_0 = 52$ mT, $z = -90$ nm, and $f = 0.1$, is plotted against T/T_C for different values of D . A d -wave temperature dependence of $\lambda(T)$ is used.³⁷ In all figures $\lambda(0) = 150$ nm.

the characteristic high field skewness with a cutoff corresponding to the field at the core of the vortices. The sharp peak corresponds to the most probable field B_{sad} at saddle points in $B(r)$ midway between adjacent vortices. The low field cutoff occurs at the center of an elementary triangle of vortices. As we move farther from the superconductor, B_{sad} moves towards the applied field as the field approaches uniformity for $z \rightarrow -\infty$, *i.e.*, $p(B) \rightarrow \delta(B - B_0)$. This crossover occurs as $\exp(\frac{2\pi}{a}z)$, as the z variation of the Fourier components $F(\mathbf{k}, z)$ in Eq. (4) is controlled by k which takes values equal to or larger than $2\pi/a$. However, if instead we consider a simple non-superconducting overlayer instead of free space, then the limiting $p(B)$ will be the intrinsic lineshape in the overlayer material.

As mentioned above $p(B)$ is also affected by disorder in the VL due to pinning at structural defects in the crystal, where the superconducting order parameter is suppressed. Such disorder causes broadening of the magnetic resonance, obscuring the features expected from an ideal VL,²⁵ adding uncertainty to parameters of interest such as λ and ξ . Relatively little is known about the detailed characteristics of this disorder. Accounting for the disorder of the VL is most often done by smearing the ideal lineshape with a Gaussian or Lorentzian distribution of width Δ_D , where the latter is a phenomenological measure of the degree of disorder.^{5,38} Calculated distributions for an applied field $B_0 = 52$ mT are shown in Fig. 1(a) for $\Delta_D = 0.3$ and 0.6 mT, together with the ideally ordered VL ($\Delta_D = 0$). Such disorder is more pronounced outside the superconductor and renders the lineshape symmetric when the depth dependent intrinsic VL broadening is smaller than Δ_D .

One major difference between conventional μSR and $\beta\text{-NMR}$ or $\text{LE-}\mu\text{SR}$ is the stopping range of the probe. In conventional μSR the μ^+ stopping range is ≈ 150 mg/cm², yielding a fraction of a mm in YBCO. In contrast, in $\beta\text{-NMR}$ or $\text{LE-}\mu\text{SR}$, the mean depth of the probe can be controlled on a nm lengthscale from the surface. For implantation depths inside the superconductor, comparable or larger than λ , the μSR lineshape (proportional to $p(B)$) is nearly field independent for $2B_{c1} \leq B_0 \leq B_{c2}$ (for $a \ll \lambda$), and the second moment of $p(B)$ follows the formula,³⁹

$$\sigma \approx \frac{0.00609\Phi_0}{\lambda^2(T)}, \quad (7)$$

neglecting the cutoff field. Using the latter makes σ slightly field-dependent, but the corrections are small for fields $B_0 \ll B_{c2}$. Outside the superconductor, the magnetic field inhomogeneity of the VL vanishes over a lengthscale that depends on the spacing between vortices, a . In particular, the recovery to a uniform field occurs on a lengthscale of $\frac{a}{2\pi}$.³¹ The field distribution is thus strongly field dependent when $a(B_0)$ is of the order of $|z|$. This is shown in Fig. 1(b), where σ due to the VL given in Eq. (6) is plotted against the applied field at a distance of 90 nm and 40 nm above the surface. In low

magnetic fields, the magnetic resonance lineshape outside the superconductor is sensitive to both the intrinsic inhomogeneity of the VL as well as any additional broadening from disorder. However, in high magnetic fields the linewidth is dominated by VL disorder.

Taking the view that the dominant source of disorder is due to twin or grain boundaries,⁴⁰ one can model the effect of disorder on the regular VL in different ways. The simplest is to assume that, in addition to the regular triangular lattice, a fraction of vortices is trapped along the structural defects such as twin or grain boundaries as shown in the inset of Fig. 1(b). The local field in real space will be the superposition of both contributions

$$B(\mathbf{r}, z) = B^{\text{vl}}(\mathbf{r}, z) + B^{\text{dis}}(\mathbf{r}, z), \\ = B_0^{\text{vl}} \sum_{\mathbf{k}} F(\mathbf{k}, z) e^{i\mathbf{k}\cdot\mathbf{r}} + B_0^{\text{dis}} \sum_{\mathbf{g}} F(\mathbf{g}, z) e^{i\mathbf{g}\cdot\mathbf{r}}, \quad (8)$$

where $B^{\text{vl}}(\mathbf{r}, z)$ is the field due to the regular VL, $B^{\text{dis}}(\mathbf{r}, z)$ the field due to the vortices pinned by disorder and \mathbf{g} is some generally incommensurate wave vector related to the pinning, which for simplicity we take to be of the form $\mathbf{g} = \frac{2\pi}{a'}n\mathbf{x} + \frac{2\pi}{D}m\mathbf{y}$, where a' is the spacing between vortices in a boundary, and D is the separation between boundaries as drawn in the inset of Fig. 1(b). The average field is then $B_0 = \sqrt{(B_0^{\text{vl}})^2 + (B_0^{\text{dis}})^2}$, where $B_0^{\text{dis}} = fB_0$ and f is the fraction of pinned vortices ($0 \leq f < 1$). The second moment of $B(\mathbf{r}, z)$ from Eq. (8) can be then easily calculated:

$$\sigma^2 = B_0^2 \left[(1 - f^2) \sum_{\mathbf{k} \neq 0} F^2(\mathbf{k}, z) + f^2 \sum_{\mathbf{g} \neq 0} F^2(\mathbf{g}, z) \right]. \quad (9)$$

It is clear from Eqs. (4) and (9), that the broadening from the VL (first term) at a distance z outside the superconductor becomes small at high magnetic fields where $|z| \gg a$. However the broadening outside the superconductor due to disorder (second term) remains large provided $|z|$ is not much larger than $\frac{D}{2\pi}$. Since D and f depend on the arrangement of twin boundaries we expect them to be sample dependent. In addition, one may also anticipate that f will decrease at high magnetic fields where the increased repulsive interaction between vortices overcomes vortex-pinning. Therefore, we assume a simplified phenomenological parameterization $f = \delta B_0^{-\gamma}$, where δ is temperature and sample dependent and $\gamma \geq 1$.

The broadening of the field distribution due to a regular VL can be significantly larger when introducing the effect of disorder due to the twin and grain boundaries. When taking the disorder into account, σ of Eq. (9) is no longer zero at high magnetic fields as seen in Fig. 1(b). This is because the broadening has a disorder component which decays on a length scale of D rather than a , where $D \gg a$ (we also assume $D \gg a'$ and thus ignore the effect of the spacing within the twin boundaries). Consequently σ shows a strong deviation from the ideal VL result as seen in Fig. 1-c as D increases. In this case the second moment from Eq. (9) no longer

scales with $1/\lambda^2$ as predicted for an ideal VL (see Eq. (7)). In particular, at low T , the broadening is almost T -independent irrespective of superconducting gap structure. It is interesting to note that the first μSR studies on powder samples of cuprates showed a very flat variation in the linewidth.^{41,42} This was taken as evidence for s -wave superconductivity. Later measurements on high quality crystals of $\text{YBa}_2\text{Cu}_3\text{O}_{7-\delta}$ showed a much different low temperature behaviour,⁴³ and, in particular, a linear variation in $1/\lambda^2(T)$ consistent with d -wave pairing.⁴⁴ Although the lineshapes in powders are expected to be more symmetric than in crystals due to the additional disorder and random orientation, the different temperature dependence is surprising since it was thought that the line broadening from disorder should also scale with $1/\lambda^2(T)$.²⁵ The current work provides a clear explanation for the discrepancy between powders and crystals. In powders, the line broadening is dominated by long wavelength pinning of vortices at grain boundaries. Consequently the resulting broadening at low temperature reflects variations in the vortex density and is thus only weakly dependent on temperature. In later work on crystals, the contribution from such long wavelength pinning is much less important. This is evident from bulk μSR in crystals where one observes the expected characteristic lineshape associated with a VL.²⁵

III. EXPERIMENTAL DETAILS

The measurements were carried out on three different near-optimally doped YBCO samples, two flux-grown single crystals and a thin film. I) The twinned single crystal in the form of a platelet ~ 0.5 mm thick with an area $\sim 2 \times 3$ mm² had $T_C = 92.5$ K. It was mechanically polished with 0.05 μm alumina, then chemically etched with a dilute (0.8%) Bromine solution followed by annealing at 200° C in dry N_2 to improve the surface quality. It was then sputter coated with a 120 nm thick Ag film (99.99 % purity) at room temperature in an Ar pressure of 30 mTorr. The deposition rate was 0.5 $\text{\AA}/\text{s}$, and to ensure Ag uniformity, the crystal was rotated. II) The optimally doped detwinned single crystal had $T_C = 92.5$ K, ~ 0.5 mm thickness, and area $\sim 3 \times 3$ mm². The crystal was cleaned, annealed, and mechanically detwinned. A 120 nm thick Ag, from the same source as above, was sputtered onto the prepared surface under similar conditions. III) The film of $T_C = 87.5$ K, critical current density $J_C = 2.10^6$ A/cm³ and 600 nm thickness, supplied by THEVA (Ismaning, Germany), was grown by thermal co-evaporation on a LaAlO_3 substrate of area 9×8 mm². The film was coated *in situ* with a 60 nm silver layer (99.99% purity).

The experiments were performed using the β -NMR spectrometer at the ISAC facility in TRIUMF, Canada, where a highly nuclear-spin-polarized beam (intensity $\sim 10^6$ ions/s) of $^8\text{Li}^+$ is produced using collinear optical pumping with circularly polarized laser light.²⁷ The

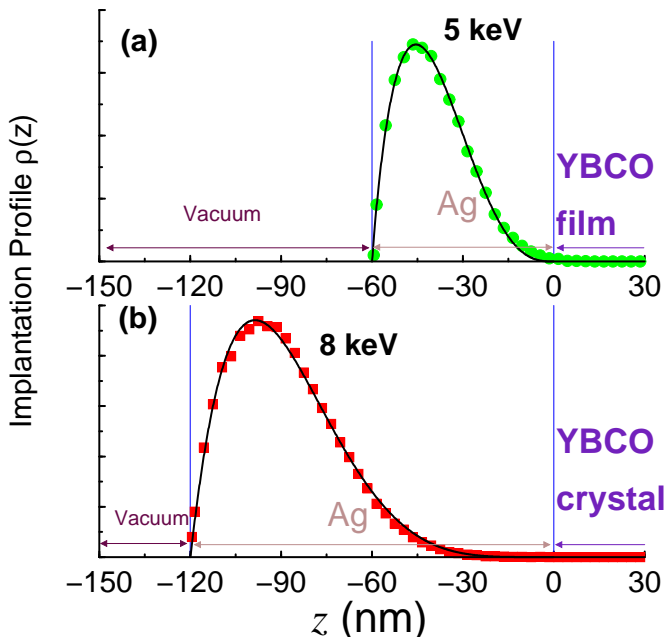


FIG. 2: (Color online) Implantation profiles of ${}^8\text{Li}^+$ at energies of (a) 5 keV into 60 nm of Ag with the mean at 40 nm away from YBCO film, and (b) 8 keV into 120 nm of Ag with the mean at 90 nm away from YBCO crystals, as calculated via TRIM.SP.⁴⁵ Solid lines are phenomenological fits.

beam is directed onto the sample which is mounted on the cold finger of a He flow cryostat and positioned in the centre of a high homogeneity superconducting solenoid. The beamline and entire spectrometer are maintained in ultrahigh vacuum (10^{-10} Torr). In β -NMR measurements, the ${}^8\text{Li}^+$ nuclear spin polarization is monitored via its asymmetric radioactive beta decay (lifetime $\tau = 1.203$ s), where the high energy (several MeV) beta electron is emitted preferentially opposite to the nuclear spin direction. The experimental asymmetry, defined as the ratio $\frac{F-B}{F+B}$ of the count rates in two plastic scintillation detectors placed in front (F) and at the back (B) of the sample, is proportional to the probe's spin polarization.^{27,28}

The whole spectrometer can be biased at high voltage, allowing one to tune the implantation energy of ${}^8\text{Li}^+$ ions and their implantation depth between 5-200 nm. Therefore, the implanted ${}^8\text{Li}^+$ can monitor the depth dependence of the local magnetic field distribution in materials at nm scale by measuring the NMR lineshape in a manner analogous to conventional NMR.^{2,28,29} In this work, the ${}^8\text{Li}^+$ ions are decelerated to stop in the Ag overlayer deposited on each of the three YBCO samples. Implantation profiles of ${}^8\text{Li}^+$ were calculated using the TRIM.SP code,⁴⁵ examples of which are shown in Fig. 2. The implantation energies used in this study (8 keV in the crystal samples and 5 keV the film), were tuned to stop all the ${}^8\text{Li}^+$ within the Ag. The mean distances are 90 and 40 nm from the Ag/YBCO interface in the crystals and film, respectively.

The β -NMR measurement is carried out by monitoring the time averaged nuclear polarization through the

beta decay asymmetry, as a function of the radio frequency (RF) ω of a small transverse oscillating magnetic field $\mathbf{B}_1 = B_1 \cos(\omega t)\hat{x}$, where $B_1 \sim 0.01$ mT. When ω matches the Larmor frequency $\omega_{\text{Li}} = \gamma_{\text{Li}} B_{\text{local}}$, where $\gamma_{\text{Li}} = 6.3015$ kHz/mT is the gyromagnetic ratio and B_{local} is the local field, the ${}^8\text{Li}^+$ spins precess about B_{local} , causing a loss of polarization. To establish the vortex state in the YBCO samples, they are cooled in a static magnetic fields $B_0 \geq B_{c1}$ applied parallel to the c -axis of YBCO (normal to the film and platelet crystals). B_0 is also parallel to both the initial nuclear spin polarization and the beam direction. The local field sensed by the ${}^8\text{Li}^+$ is determined by the applied field and the internal magnetic field generated by the screening currents associated with the vortex lattice. Thus, B_{local} is distributed over a range of values, which can be calculated using

$$p(B) = \int_{-d}^0 dz \rho(z) \frac{1}{A} \int_A dr \delta(B - B(\mathbf{r}, z)). \quad (10)$$

where $\rho(z)$ is the implantation profile calculated using TRIM.SP given in Fig. 2.

When ${}^8\text{Li}^+$ is implanted in Ag (with no superconducting substrate) at temperatures below 100 K, it exhibits a single narrow resonance at the Larmor frequency.²⁸ The resonance should yield an approximately Gaussian distribution caused by nuclear dipolar moments.⁴⁶ However, continuous wave RF leads to a power-broadened Lorentzian lineshape, whose linewidth is small (1 kHz ≈ 0.15 mT) and corresponds to the dipolar broadening due to the ${}^{107,109}\text{Ag}$ nuclear moments and RF power broadening.⁴⁷ In the presence of any additional magnetic inhomogeneity in the Ag, due for example to a VL associated with a superconducting substrate, the observed resonance lineshape will be a convolution of the narrow RF power broadened Lorentzian of Ag with the (depth dependent) field distribution due to the VL in the substrate. There are unique aspects of measuring the field distribution in the Ag overlayer compared to the superconductor itself. As mentioned above, in high magnetic field, it is possible to isolate and study the broadening due to VL disorder that occurs on a long length scale. Also in low magnetic fields, where the broadening is dominated by the VL, it should be possible to measure λ in magnetic superconductors since the field distribution above the sample is free of any internal hyperfine fields that make a bulk measurement impossible.³²

IV. RESULTS

The β -NMR resonances were measured as a function of temperature under field-cooled conditions at fields ranging from $B_0 = 20$ mT to 3.3 T in each one of the three samples. Fig. 3, shows typical resonance lineshapes at various temperatures in sample I with $B_0 = 51.7$ mT. Above T_C , the line broadening is small and temperature

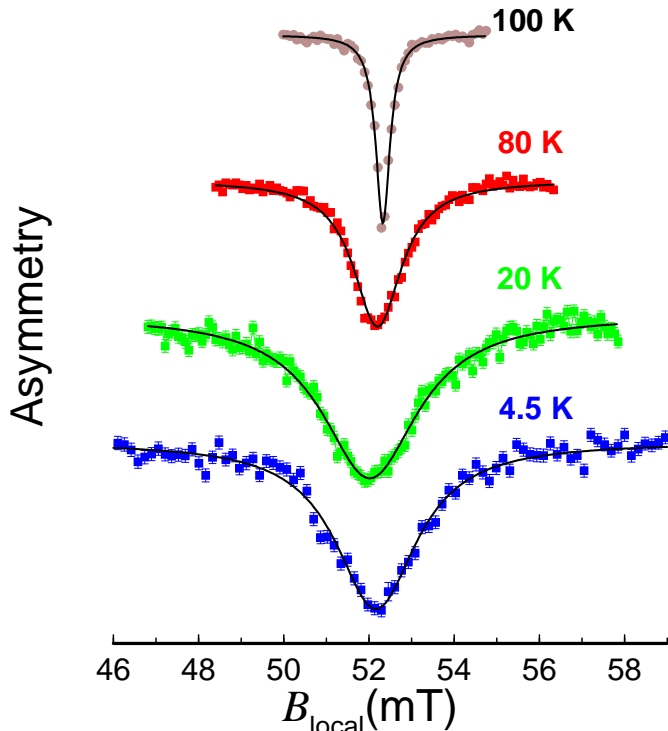


FIG. 3: (Color online) β NMR resonances in Ag/YBCO (crystal I) at temperatures 100 K, 80 K, 20 K, and 4.5 K measured in a magnetic field B_0 of 52.3 mT applied along YBCO c -axis. The solid lines are best fits using a Lorentzian.

independent as expected from nuclear dipolar broadening. Below T_C , the field distribution in the Ag overlayer broadens dramatically from the VL in the underlying superconductor. Such broadening was observed in all samples and at all magnetic fields, although there are significant variations as a function of both magnetic field and sample as discussed below. The first thing to note is that the lineshape is very symmetric and fits well to a simple Lorentzian. This is much different from the asymmetric lineshape observed with conventional μ SR in samples similar to I and II.^{25,43} The other significant difference between the current results and previous bulk μ SR measurements^{4,9,25,43} on crystals is that the broadening at low temperatures is only weakly dependent on temperature, as may be seen by comparing the resonances at 20 K and 4.5 K. In contrast, the broadening from an ordered VL lattice scales with $1/\lambda^2$ and consequently in YBCO shows a strong linear T -dependence at low temperatures due to the d -wave superconducting order.^{43,44}

The observed lineshape fits well to a convolution of two Lorentzians, one from vortices in the superconducting state with a full width at half maximum (FWHM) Δ_{sc} , and one from other sources determined from the normal state of FWHM Δ_{ns} . The width of a convolution of two Lorentzians is the sum of the individual widths: $\Delta(T) = \Delta_{sc}(T) + \Delta_{ns}$. Therefore, the contribution from

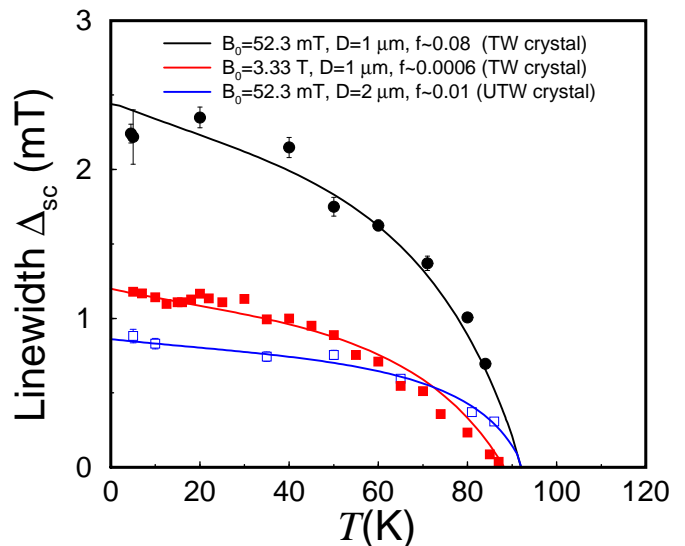


FIG. 4: (Color online) The vortex-related broadening below T_C , $\Delta_{sc}(T) = \Delta(T) - \Delta_{ns}$ of the twinned (full symbols) and detwinned (opaque squares) YBCO crystals in an applied field B_0 . $\Delta(T)$ is the linewidth at temperature T of the Lorentzian fits and Δ_{ns} is the constant linewidth in the normal state. Solid lines represent a fit using $\Delta_{DVL} = 2.355\sigma$ where σ is given in Eq. (9) and D and f are varied to fit the data. A d -wave temperature dependence of $\lambda(T)$ in YBCO is used,³⁷ where $\lambda(0) = 150$ nm.

vortices in the superconducting state can be obtained by simply subtracting the temperature independent normal state width. Fig. 4 shows the resulting $\Delta_{sc}(T)$ as one enters the superconducting state in samples I and II. At low field, the measured width (~ 2.2 mT) at low temperature is larger than expected from a regular VL and decreases significantly in the detwinned crystal to about ~ 0.6 mT. For comparison, simulations using Eq. (10) and the $^8\text{Li}^+$ stopping profile in Fig. 2(b); indicate that the broadening due to a regular VL is only $\Delta_{VL} \sim 0.3$ mT. At 3.33 T, the discrepancy between the observed width (see Fig. 4) and that expected from a regular VL is even more dramatic. At this high field the vortices are spaced so closely ($a \approx 27$ nm), that there should be no detectable broadening from a regular VL for our stopping depths. This can be seen clearly from the simulation in Fig. 1(b), where the VL broadening approaches zero at high fields. In contrast, the data at 3.33 T shows significant broadening below T_C which is therefore solely attributed to vortex disorder on a long length scale.

The temperature dependence of the broadening is also much weaker than expected from a regular VL in YBCO, where $1/\lambda^2$ has a strong linear term due to the d -wave order parameter.^{43,44} The observed temperature dependence fits well to our model of disorder, where $\Delta_{sc}(T)$ is compared to an estimate of the FWHM given by $\Delta_{DVL} \approx 2.355\sigma$, where σ is given in Eq. (9). This leads to an estimate of D of the order of a micron, consistent

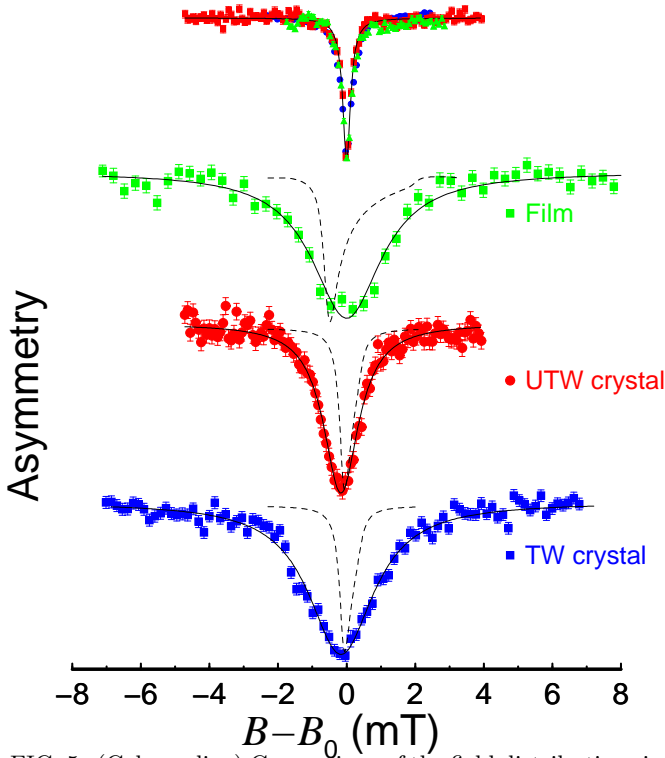


FIG. 5: (Color online) Comparison of the field distributions in the three samples taken at temperatures 100 K (top panel), 5 K (crystals) and 10 K (film). The x-axis is shifted by B_0 , the applied field which is 52.3 (51.7) mT for the crystals (film). Solid lines are Lorentzian fits and dashed lines are the simulation described in the text.

with the the separation between twin boundaries or grain boundaries.⁴⁸ In the detwinned crystal, D is found to be larger but not infinite since the detwinning is not complete. The fraction of vortices f pinned by structural defects in the twinned crystal is about ~ 0.1 at low field (52 mT) and decreases considerably at high field (3.33 T). Thus, the amplitude of the enhanced vortex density at the defects, fB_0 , varies between 2-4 mT at all fields. In the detwinned crystal, $f \sim 0.01$, is an order of magnitude smaller than in the twinned crystal at the same field, with small variation in the vortex density (0.5 mT) compared to the twinned crystal. These results are consistent with expectations from pinning at twin boundaries. In particular, one expects the fraction of vortices pinned will decrease in the partially detwinned crystals. Also, it is reasonable to expect that in a high magnetic fields the fraction of vortices pinned will decrease due to the smaller separation between vortices and resulting increase in the repulsive interaction.

In Fig. 5, the spectra in all three samples above and below T_C are compared with the corresponding simulated field distributions. The observed lineshapes are all symmetric, and significantly broader than expected, showing little or no sign of the characteristic VL field distribution. Simulation of the VL lineshapes (dashed lines) was done using Eqs. (4), (5), and (10), for $\lambda = 150$ nm, and

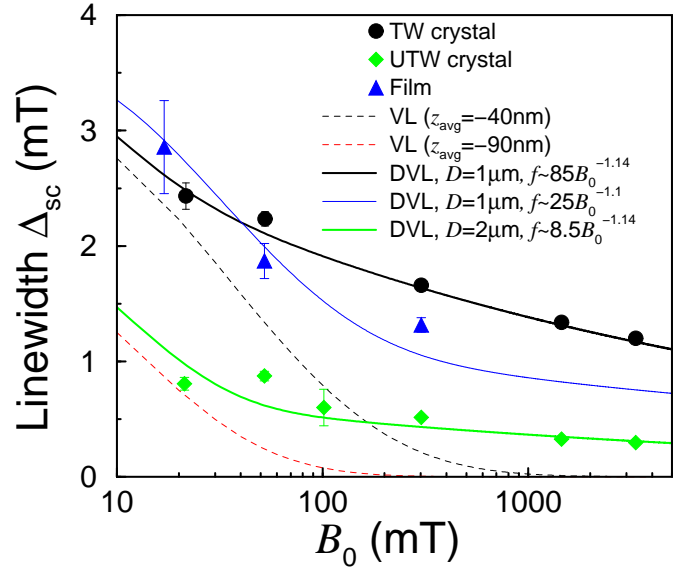


FIG. 6: (Color online) Superconducting broadening $\Delta_{sc}(T)$ of the β -NMR resonance spectra at temperatures ~ 4.5 -10 K in the three samples. The experimental broadening is compared with the linewidth of an ideal VL Δ_{VL} (dashed lines), and Δ_{DVL} of a disordered VL (solid lines), which are both weighted by the ${}^8\text{Li}^+$ profile given in Fig. 2.

was convoluted with a Lorentzian representing the normal state spectra with $\Delta_{ns} = 0.3$ mT. The theoretical lineshape for the film is broader and asymmetric because it is weighted by the ${}^8\text{Li}^+$ stopping distribution which was on average closer to the superconductor. The lineshapes for the crystals are almost symmetric as the ideal VL lineshape at the depths of an average 90 nm away from the superconductor are narrower than the Lorentzian they are convoluted with. The magnetic field dependence of the superconducting linewidth $\Delta_{sc}(T)$ at low temperatures ~ 4.5 -10 K is plotted in Fig. 6. In all samples, we find that the broadening is largest at low field and decreases gradually with increasing field. Also, in all cases the broadening remains large and well above the prediction from a regular VL, approximated by $\Delta_{VL} \approx 2.355\sigma$ where σ of an ideal VL is given in Eq. (6) and weighted by the ${}^8\text{Li}^+$ profile given in Fig. 2. The broadening is substantially smaller in the detwinned crystal compared to the other samples. One can account for all of the data using a linewidth due to a disordered VL, $\Delta_{DVL} \approx 2.355\sigma$, where σ is now given in Eq. (9)) and weighted by the ${}^8\text{Li}^+$ profile plotted in Fig. 2. The data is well fitted (see Fig. 6) by assuming that the twin/grain boundaries spacing D is sample dependent of the order of a few microns, and by assuming a phenomenological form for the fraction of pinned vortices $f = \delta B_0^{-\gamma}$ with $\gamma \sim 1.1$ and δ sample dependent.

V. DISCUSSION AND CONCLUSIONS

It is clear that the β -NMR lineshapes in the Ag overlayer differ substantially from that expected from a well-ordered VL field distribution. This has little to do with the method of observation. For example, in the conventional superconductor NbSe₂, β -NMR shows the expected VL lineshape.² The lineshapes reported here in the YBCO film are also qualitatively different than that seen with LE- μ SR in a YBCO film coated with a 60 nm thick Ag layer.³⁶ In that experiment the authors found a more asymmetric lineshape in the Ag overlayer which was closer to that of a regular VL. Some of this difference may be due to the different pinning characteristics of the samples, although the YBCO film used by Niedermayer *et al.* was from the same source as sample III. Also, the LE- μ SR experiment was probing the VL closer to the interface and in a lower applied field where the disorder is less important compared to the contribution from the ordered VL. The symmetry and large broadening of the lineshape at low fields cannot be accounted for by VL melting (at a reentrant vortex liquid state near B_{c1}) which would instead yield a motional narrowing of the field distribution.⁴⁹

The observed resonances in the current experiment are dominated by long range variations of the vortex density across the face of the sample.¹⁸ Such disorder in the VL can produce a symmetric lineshape,^{38,50} and can broaden the field distribution significantly compared to that of the corresponding ordered state.⁵¹ Weak random pinning or point-like disorder due to oxygen deficiency may slightly distort the VL, and may also broaden the lineshape.³⁹ However, the correlated disorder due to the twin and grain boundaries is dominant at long wavelengths,^{40,52} and therefore we are mostly sensitive to the twin/grain boundaries. Indeed, the position of the probe outside the superconductor enhances its sensitivity to long wavelength disorder, as the proximal fields fall off with distance as $\exp(-2\pi|z|/D)$ where D is the wavelength of the inhomogeneity of the field.⁵³ The broadening is reduced in a detwinned crystal where the twin boundaries are more sparse as shown in Fig. 5, thus the vortex density variation across the face of the sample is smaller than in the twinned crystals as f is largely reduced.

The extrinsic broadening due to disorder at low temperature, $\Delta_D = \Delta_{sc} - \Delta_{VL}$, reported here is between 0.5 mT and 2.5 mT. This is remarkably close to the additional Gaussian broadening required to explain lineshapes in bulk μ SR measurements on crystals.^{25,38,54} In the bulk, this extrinsic broadening is small compared to the intrinsic VL broadening, whereas outside the sample the reverse is true. It is important to note the T -dependence of the extrinsic broadening in Fig. 4 *does not follow the superfluid density* ($\propto 1/\lambda^2$) which

varies linearly at low- T because of the d -wave order parameter.^{44,55} Instead, we observe a much weaker T -dependence. This is expected from our model of disorder which occurs on a long length scale D . For example, at low- T where λ is short compared to D , the flux density outside the sample is determined solely by inhomogeneities in the vortex density, and is independent of the superfluid density as the vortices are static and well-pinned in the twin boundaries. The current results may also explain early μ SR work on HTSC powders and sintered samples which mistakenly indicated an s -wave T -dependence of $1/\lambda^2$.^{41,42} It is likely in these cases the linewidth was dominated by extrinsic VL disorder on a long length scale. This tends to flatten the T -dependence of the linewidth and the effective λ obtained from the analysis.^{41,56} Therefore we conclude that although the linewidth obtained from powders can be useful in making rough estimates of λ , one cannot extract accurate measurements of λ or its T -dependence without additional information about the source of broadening and in particular VL disorder.

In conclusion, we have measured the magnetic field distributions due to the vortex state of YBCO using β -NMR. We find a significant inhomogeneous broadening of the NMR attributed to the underlying VL in YBCO. However, the observed resonances have several unexpected properties. In particular, they are broader and more symmetric than for an ideal VL. The anomalous broadening is most evident in high field where there is no significant contribution from the regular VL. These effects are attributed to long wavelength disorder from pinning at twin or grain boundaries. The temperature dependence of the disorder-related broadening does not scale with $1/\lambda^2$, suggesting there is a contribution to the linewidth in the bulk of the vortex state that does not track the superfluid density. This is likely to have only a minor effect on the interpretation of data on crystals where the observed lineshape is close to that expected from a well ordered VL. However, it can be significant in powders or crystals where there is substantial disorder in the VL. In particular, when the broadening is dominated by VL disorder on a long length scale (i.e. much bigger than λ) the temperature dependence of the linewidth does not scale with $1/\lambda^2$ and therefore cannot be used to determine the symmetry of the superconducting gap.

Acknowledgments

We would like to thank D. A. Bonn, W. N. Hardy, and R. Liang for providing the YBCO crystals. We would also like to acknowledge R. Abasalti, D. Arseneau, and S. Daviel for expert technical support, and NSERC, CIFAR for financial support.

* Present address: LMU PSI, Villigen CH.

¹ E. H. Brandt, J. Low Temp. Phys. **139**, 21 (2005).

- ² Z. Salman, D. Wang, K. H. Chow, M. D. Hossain, S. Kretitzman, T. A. Keeler, C. D. P. Levy, W. A. MacFarlane, R. I. Miller, G. D. Morris, T. J. Parolin, H. Saadaoui, M. Smadella, and R. F. Kiefl, *Phys. Rev. Lett.* **98**, 167001 (2007).
- ³ R. Khasanov, A. Shengelaya, A. Maisuradze, F. La Mattina, A. Bussmann-Holder, H. Keller, and K. A. Müller, *Phys. Rev. Lett.* **98**, 057007 (2007).
- ⁴ J. E. Sonier, S. A. Sabok-Sayr, F. D. Callaghan, C. V. Kaiser, V. Pacradouni, J. H. Brewer, S. L. Stubbs, W. N. Hardy, D. A. Bonn, Ruixing Liang, and W. A. Atkinson, *Phys. Rev. B* **76**, 134518 (2007).
- ⁵ E. H. Brandt, *J. Low Temp. Phys.* **73**, 355 (1988).
- ⁶ Y. M. Belousov and V. P. Smilga, *Spectroscopy of High-Tc Superconductors: A Theoretical View* By N. M. Plakida, page 236-292, CRC Press (2003).
- ⁷ R. I. Miller, R. F. Kiefl, J. H. Brewer, J. E. Sonier, J. Chakhalian, S. Dunsiger, G. D. Morris, A. N. Price, D. A. Bonn, W. H. Hardy, and Ruixing Liang, *Phys. Rev. Lett.* **88**, 137002 (2002).
- ⁸ M. H. S. Amin, I. Affleck, and M. Franz, *Phys. Rev. B* **58**, 5848 (1998).
- ⁹ J. E. Sonier, J. H. Brewer, R. F. Kiefl, G. D. Morris, R. I. Miller, D. A. Bonn, J. Chakhalian, R. H. Heffner, W. N. Hardy, and R. Liang, *Phys. Rev. Lett.* **83**, 4156 (1999).
- ¹⁰ M. Franz, C. Kallin, P. I. Soininen, A. J. Berlinsky, and A. L. Fetter, *Phys. Rev. B* **53**, 5795 (1996).
- ¹¹ M. H. S. Amin, M. Franz, and I. Affleck, *Phys. Rev. Lett.* **84**, 5864 (2000).
- ¹² H. Hilgenkamp, and J. Mannhart, *Rev. Mod. Phys.* **74**, 485 (2002).
- ¹³ G. Blatter, M. V. Feigel'man, V. B. Geshkenbein, A. I. Larkin and V. M. Vinokur, *Rev. Mod. Phys.* **66**, 1125 (1994).
- ¹⁴ D.J. Bishop, P. L. Gammel, D. A. Huse, and C. A. Murray, *Science* **255**, 165 (1992).
- ¹⁵ M. Yethiraj, H. A. Mook, G. D. Wignall, R. Cubitt, E. M. Forgan, D. M. Paul, and T. Armstrong, *Phys. Rev. Lett.* **70**, 857 (1993).
- ¹⁶ P. L. Gammel, D. J. Bishop, G. J. Dolan, J. R. Kwo, C. A. Murray, L. F. Schneemeyer, and J. V. Waszczak, *Phys. Rev. Lett.* **59**, 2592 (1987).
- ¹⁷ J. A. Herbsommer, G. Nieva, and J. Luzuriaga, *Phys. Rev. B* **61**, 11745 (2000).
- ¹⁸ I. Maggio-April, C. Renner, A. Erb, E. Walker, and Ø. Fisher, *Nature* **390**, 487 (1997).
- ¹⁹ Ch. Simon, A. Pautrat, G. Poullain, C. Goupil, C. Leblond-Harnois, X. Chaud, and A. Brulet, *Phys. Rev. B* **70**, 024502 (2004).
- ²⁰ D. S. Fisher, M. P. A. Fisher, and D. A. Huse, *Phys. Rev. B* **43**, 130 (1991).
- ²¹ D. R. Nelson and V. M. Vinokur, *Phys. Rev. Lett.* **68**, 2398 (1992).
- ²² G. P. Mikitik, and E. H. Brandt, *Phys. Rev. B* **79**, 020506(R) (2009).
- ²³ For example, see E. Bartolomé, B. Bozzo, X. Granados, F. Sandiumenge, T. Puig, and X. Obradors, *Supercond. Sci. Technol.* **21**, 125002 (2008), and references there in.
- ²⁴ A. Rigamonti, F. Borsa, and P. Carretta, *Rep. Prog. Phys.* **61**, 1367 (1998), and references there in.
- ²⁵ J. E. Sonier, J. H. Brewer, and R. F. Kiefl, *Rev. Mod. Phys.* **72**, 769 (2000), and references there in.
- ²⁶ E. Morenzoni, Physics and applications of low energy muons, in *Muon Science*, S. Lee *et al.* Eds., IOP Publishing, Bristol (1999).
- ²⁷ R. F. Kiefl, W. A. MacFarlane, G. D. Morris, P. Amaudruz, D. Arseneau, H. Azumi, R. Baartman, T. R. Beals, J. Behr, C. Bommas, J. H. Brewer, K. H. Chow, E. Dumont, S. R. Dunsiger, S. Daviel, L. Greene, A. Hatakeyama, R. H. Heffner, Y. Hirayama, B. Hitti, S. R. Kretitzman, C. D. P. Levy, R. I. Miller, M. Olivo, and R. Poutissou, *Physica B* **326**, 189 (2003).
- ²⁸ G. D. Morris, W. A. MacFarlane, K. H. Chow, Z. Salman, D. J. Arseneau, S. Daviel, A. Hatakeyama, S. R. Kretitzman, C. D. P. Levy, R. Poutissou, R. H. Heffner, J. E. Elenewski, L. H. Greene, and R. F. Kiefl, *Phys. Rev. Lett.* **93**, 157601 (2004).
- ²⁹ Z. Salman, E. P. Reynard, W. A. MacFarlane, K. H. Chow, J. Chakhalian, S. R. Kretitzman, S. Daviel, C. D. P. Levy, R. Poutissou, and R. F. Kiefl, *Phys. Rev. B* **70**, 104404 (2004).
- ³⁰ Z. Salman, K. H. Chow, R. I. Miller, A. Morello, T. J. Parolin, M. D. Hossain, T. A. Keeler, C. D. P. Levy, W. A. MacFarlane, G. D. Morris, H. Saadaoui, D. Wang, R. Sessoli, G. G. Condorelli, and R. F. Kiefl, *Nano Lett.* **7**, 1551 (2007).
- ³¹ M. Xu, M. D. Hossain, H. Saadaoui, T. J. Parolin, K. H. Chow, T. A. Keeler, R. F. Kiefl, G. D. Morris, Z. Salman, Q. Song, D. Wang, and W. A. MacFarlane, *Journal of Magnetic Resonance* **191**, 47 (2008).
- ³² H. Saadaoui, W. A. MacFarlane, G. D. Morris, Z. Salman, K. H. Chow, I. Fan, M. D. Hossain, R. Liang, A. I. Mansour, T. J. Parolin, M. Smadella, Q. Song, D. Wang, and R. F. Kiefl *Physica B* **404**, 730 (2009).
- ³³ C. P. Poole Jr., H. A. Farch, and R. J. Creswick, *Superconductivity, Academic Press. Inc.* (1995).
- ³⁴ M. Požek, H. U. Habermeier, A. Maier, and M. Mehring, *Physica C* **269**, 61 (1996).
- ³⁵ A. Steegmans, R. Provoost, R. E. Silverans, and V. V. Moshchalkov, *Physica C* **302**, 159 (1998).
- ³⁶ Ch. Niedermayer, E. M. Forgan, H. Glückler, A. Hofer, E. Morenzoni, M. Pleines, T. Prokscha, T. M. Riseman, M. Birke, T. J. Jackson, J. Litterst, M. W. Long, H. Luetkens, A. Schatz, and G. Schatz, *Phys. Rev. Lett.* **83**, 3932 (1999).
- ³⁷ Microwave data courtesy of D. A. Bonn.
- ³⁸ D. R. Harshman, E. H. Brandt, A. T. Fiory, M. Inui, D. B. Mitzi, L. F. Schneemeyer and J. V. Waszczak, *Phys. Rev. B* **47**, 2905 (1993).
- ³⁹ E. H. Brandt, *Phys. Rev. B* **37**, 2349 (1988), and E. H. Brandt, *Phys. Rev. Lett.* **66**, 3213 (1991).
- ⁴⁰ D. R. Nelson and V. M. Vinokur, *Phys. Rev. B* **48**, 13060 (1993).
- ⁴¹ D. R. Harshman, G. Aeppli, E. J. Ansaldo, B. Batlogg, J. H. Brewer, J. F. Carolan, R. J. Cava, M. Celio, A. C. D. Chaklader, W. N. Hardy, S. R. Kretitzman, G. M. Luke, D. R. Noakes, and M. Senba, *Phys. Rev. B* **36**, 2386 (1987).
- ⁴² R. F. Kiefl, T. M. Riseman, G. Aeppli, E. J. Ansaldo, J. F. Carolan, R. J. Cava, W. N. Hardy, D. R. Harshman, N. Kaplan, J. R. Kempton, S. R. Kretitzman, G. M. Luke, B. X. Yang, and D. Ll. Williams, *Physica C* **153**, 757 (1988).
- ⁴³ J. E. Sonier, R. F. Kiefl, J. H. Brewer, D. A. Bonn, J. F. Carolan, K. H. Chow, P. Dosanjh, W. N. Hardy, Ruixing Liang, W. A. MacFarlane, P. Mendels, G. D. Morris, T. M. Riseman, and J. W. Schneider, *Phys. Rev. Lett.* **72**, 744 (1994).
- ⁴⁴ W. N. Hardy, D.A. Bonn, D. C. Morgan, R. Liang, and K. Zhang *Phys. Rev. Lett.* **70**, 3999 (1993).
- ⁴⁵ W. Eckstein, *Computer Simulation of Ion-Solid Interac-*

- tions (Springer, Berlin, 1991).
- ⁴⁶ A. Abragam, *Principles of Nuclear Magnetism* (Oxford University Press, Oxford, 1961).
- ⁴⁷ T. J. Parolin, Z. Salman, K. H. Chow, Q. Song, J. Valiani, H. Saadaoui, A. OHalloran, M. D. Hossain, T. A. Keeler, R. F. Kiefl, S. R. Kreitzman, C. D. P. Levy, R. I. Miller, G. D. Morris, M. R. Pearson, M. Smadella, D. Wang, M. Xu, and W. A. MacFarlane *Phys. Rev. B* **77**, 214107 (2008).
- ⁴⁸ G. J. Dolan, G. V. Chandrashekhar, T. R. Dinger, C. Feild, and F. Holtzberg *Phys. Rev. Lett.* **62**, 827 (1989);
- ⁴⁹ S. L. Lee, P. Zimmermann, H. Keller, M. Warden, I. M. Savić, R. Schauwecker, D. Zech, R. Cubitt, E. M. Forgan, P. H. Kes, T. W. Li, A. A. Menovsky, and Z. Tarnawski, *Phys. Rev. Lett.* **71**, 3862 (1993).
- ⁵⁰ U. Divakar, A. J. Drew, S. L. Lee, R. Gilardi, J. Mesot, F. Y. Ogrin, D. Charalambous, E. M. Forgan, G. I. Menon, N. Momono, M. Oda, C. D. Dewhurst, and C. Baines, *Phys. Rev. Lett.* **92**, 237004 (2004).
- ⁵¹ A. V. Minkin and S. L. Tsarevsii, *Phys. Sol. Sta.* **46**, 420 (2004).
- ⁵² E. Olive and E. H. Brandt, *Phys. Rev. B* **57**, 13861 (1998).
- ⁵³ N. Bontemps, D. Davidov, P. Monod, and R. Even, *Phys. Rev. B* **43**, 11512 (1991).
- ⁵⁴ T. M. Rise-man, J. H. Brewer, K. H. Chow, W. N. Hardy, R. F. Kiefl, S. R. Kreitzman, R. Liang, W. A. MacFarlane, P. Mendels, G. D. Morris, J. Rammer, J. W. Schneider, C. Niedermayer, and S. L. Lee, *Phys. Rev. B* **52**, 10569 (1995).
- ⁵⁵ Y. J. Uemura, G. M. Luke, B. J. Sternlieb, J. H. Brewer, J. F. Carolan, W. N. Hardy, R. Kadono, J. R. Kempton, R. F. Kiefl, S. R. Kreitzman, P. Mulhern, T. M. Rise-man, D. Ll. Williams, B. X. Yang, S. Uchida, H. Takagi, J. Gopalakrishnan, A. W. Sleight, M. A. Subramanian, C. L. Chien, M. Z. Cieplak, G. Xiao, V. Y. Lee, B. W. Statt, C. E. Stronach, W. J. Kossler, and X. H. Yu, *Phys. Rev. Lett.* **62**, 2317 (1989).
- ⁵⁶ B. Pümpin, H. Keller, W. Kündig, W. Odermatt, I. M. Savić, J. W. Schneider, H. Simmler, and P. Zimmermann, E. Kaldis and S. Rusiecki, Y. Maeno and C. Rossel, *Phys. Rev. B* **42**, 8019 (1990).

